JOURNAL OF MATERIALS SCIENCE 32 (1997) 3427–3433

Evaluation of subgrain formation in Al_2O_3–SiC nanocomposites

JIANXIN FANG, M. P. HARMER, H. M. CHAN
Department of Materials Science and Engineering and Materials Research Center, Lehigh University, Bethlehem, PA 18015, USA

Both theoretical analysis and transmission electron microscopy (TEM) complementary studies have been conducted to evaluate the possible role of subgrain formation as a strengthening mechanism in a nanocomposite consisting of Al_2O_3 and 5 vol % 0.15 μm SiC particles. The theoretical calculation predicted that the residual stresses due to thermal expansion mismatch between Al_2O_3 and SiC are insufficient to induce the extensive plastic deformation required for subgrain formation upon annealing. This prediction was consistent with TEM observations that the bulk of the material was completely free from subgrains, and that only a low density of dislocations was present in isolated areas. The results suggest, therefore, that microstructure refinement through subgrain formation cannot account for the superior mechanical behaviour of the nanocomposite reported in previous studies.

TEM examination of the ground surfaces revealed significant plastic deformation in both single phase Al_2O_3 and the nanocomposite. Upon annealing at 1300 °C for 2 h, dislocation-free subgrains were formed in Al_2O_3, whereas a high density of tangled dislocations were present in the nanocomposite. These observed differences are consistent with the fact that during annealing, residual stress relaxation is more difficult in the nanocomposite than in Al_2O_3.

1. Introduction

Niihara *et al.* [1–3] were the first to demonstrate that the incorporation of submicron SiC particles can significantly improve the mechanical behaviour of Al_2O_3. Specifically, the addition of as little as 5 vol % 0.3 μm SiC not only increased the unindented strength from 380 to 1000 MPa, but also improved the toughness from 3.25 to 4.7 MPa $m^{1/2}$. Thermal annealing at 1300 °C for 2 h further enhanced the nanocomposite strength to over 1500 MPa. Subsequently, Zhao *et al.* [4] studied the room-temperature mechanical behaviour of this system. These workers confirmed that the nanocomposite exhibited superior mechanical properties compared with Al_2O_3, but only when both materials had been hot pressed and subjected to industrial machining and subsequent annealing. Annealing for 2 h at 1300 °C increased the unindented strength of the nanocomposite from 760 to 1000 MPa. In contrast, the apparent toughness of the nanocomposite (derived from indented strength values) slightly *decreased* after annealing, although it was still higher than the toughness of the machined/annealed Al_2O_3.

As well as the discrepancy between the reported magnitude of mechanical property improvement attainable in the nanocomposite materials [1, 4–6], uncertainty remains over the mechanism(s) behind the beneficial effects of the SiC particles and the subsequent annealing treatment. One interpretation [7, 8] is that the strengthening effects are largely due to microstructure refinement through subgrain formation. In this mechanism, it is proposed that local residual stresses, due to the mismatch of thermal expansion coefficients between Al_2O_3 and SiC, are sufficiently large to generate a high density of dislocations in the Al_2O_3 matrix. During sintering, the dislocations pin and pile up at SiC particles to form networks, which in turn evolve into sub-grain boundaries. These sub-grain boundaries become more extensive after annealing, resulting in the refinement of matrix Al_2O_3 grains.

In contrast, Zhao *et al.* [4] have argued that the improved mechanical behaviour in the nanocomposite comes from surface compressive residual stresses developed during the machining process. They proposed that on annealing, the intrinsic strength in the nanocomposite increases due to the healing of machining-induced cracks. Further, in the nanocomposite, most of the apparent toughening is retained upon annealing because the surface residual stresses are only partially relaxed. The implicit hypothesis in this argument is that during annealing of the nanocomposite, cracks are able to heal more easily, but that residual stress relaxation is more difficult. A recent study by Thompson *et al.* [9] has indeed shown that upon annealing, indentation-induced cracks *healed* in the nanocomposite, but cracks *grew* in single phase Al_2O_3. Furthermore, employing a novel indentation technique, Fang *et al.* [10] provided

0022–2461

strong evidence that annealing at 1300 °C for 2 hours *completely* relaxed residual stresses in single phase alumina, but only *partially* relieved the stresses in the nanocomposite.

One objective of the present work was to test the subgrain formation hypothesis using two approaches. The first approach was to calculate the maximum theoretical residual stresses that could arise due to thermal expansion mismatch, and then to compare the magnitude of these stresses with those required to activate different types of dislocation motion in alumina. In the second approach, transmission electron microscopy (TEM) was employed to directly observe the dislocation structure within the interior of the nanocomposite. In addition, it was decided to investigate the microscopic mechanism for the difference in the residual stress recovery between Al_2O_3 and the nanocomposite. For this purpose, TEM was again applied to examine the ground surfaces under both unannealed and annealed conditions. The overall goal of the present work, therefore, was to shed light on the strengthening mechanism in nanocomposite materials.

2. Experimental procedure

Materials used in the current study were single phase Al_2O_3 and nanocomposite consisting of Al_2O_3 and 5 vol % 0.15 μm SiC prepared using hot pressing and pressureless sintering. One group of nanocomposites was annealed at 1300 °C for 2 h in an argon atmosphere. Details of material preparation have been reported elsewhere [11].

The microstructure within the interior of the samples was characterized on both hot-pressed and pressureless-sintered nanocomposites. Slices (thickness ~500 μm thick) were cut using a low-speed diamond saw from bulk samples and ground to 200 μm using a diamond grinding wheel. Discs (~3 mm diameter) were ultrasonically cut from the slices, and further reduced to about 100 μm by sequentially grinding and polishing down to a 1 μm finish. The disks were further dimpled from one side to a thickness of ~50 μm using 0.03 μm diamond paste. Finally, thin foils were prepared by ion-beam thinning the discs from both sides at a voltage of 4.5 kV and an incident beam angle of 12.5°.

The microstructure characterization of the ground surface was carried out for the hot-pressed single phase Al_2O_3 and the nanocomposite. Bulk samples of these two materials were simultaneously ground with 15 μm diamond compound. Each sample was cut into two pieces, one of which was subsequently annealed at 1300 °C for 2 h in flowing argon. TEM thin foils were prepared following the procedure described above. In order to retain the original polished surface, however, each thinning step was carried out from only one side.

Some difficulty was encountered in preparing thin foils containing the machined surface. During ion-beam thinning, thinned central regions began to bow out (the original mechanically machined surface always on the convex side). On further thinning, radial cracks initiated and were arrested within the thicker surrounding regions. Because of the afore-mentioned severe bending and cracking, only limited regions of sample which were electron transparent could be obtained. Upon annealing at 1300 °C for 2 h, bending and cracking still occurred in the nanocomposite, but not in Al_2O_3. From the above observations we can infer that machining introduces compressive residual surface stresses, and that annealing relaxes the residual stresses almost entirely in Al_2O_3, but only partially in the nanocomposite.

Following carbon coating, all thin foils were examined using a Phillips EM 400 scanning transmission electron microscope operated at an accelerating voltage of 120 kV.

3. Results and discussion

3.1. Residual stress calculation

For materials containing a particulate second phase, on cooling from the processing temperature, residual stresses will be developed due to differences in the thermal expansion and elastic constants between the matrix and the particle. Assuming that the particle is spherical, residual stresses in the matrix can be described by the following well-established equation derived by Selsing [12]

$$\sigma_{rr} = -2\sigma_{\theta\theta} = -\left(\frac{R}{r}\right)^3 \int_T^{T_R} \frac{\alpha_m - \alpha_p}{(1+\nu_m)/2E_m + (1-2\nu_p)/E_p}\, dT \quad (1)$$

where σ_{rr} is the radial compressive and $\sigma_{\theta\theta}$ the tangential tensile component of the matrix stress. R is the radius of the particle and r the distance from the centre of the particle. The parameters α_m, α_p, ν_m, ν_p, E_m and E_p are the thermal expansion coefficients, Poisson's ratios and Young's moduli of the matrix and particle, respectively. Equation 1 is a modified form of Selsing's equation based on the assumption that α_m, α_p, E_m, E_p, ν_m and ν_p are constant through the cooling temperature range. Equations describing the temperature dependence of these materials parameters are listed in Table I. T is the temperature of interest on cooling down from the processing temperature, and T_R is the temperature above which the stresses are completely relaxed through creep processes. In previous studies involving thermal residual stresses in Al_2O_3/SiC composites [16–19], designated values of T_R range from 1000 to 1250 °C. This choice of T_R is consistent with the experimental measurement of residual thermal strain in a composite of Al_2O_3 reinforced with SiC whiskers by Majumdar *et al.* [20, 21] using a neutron diffraction technique. These workers found that the residual strain within the SiC whiskers significantly reduced with increasing temperature up to 1000 °C, and approached a value of zero at about 1250 °C when extrapolated linearly. In the present calculation, the upper limit temperature was used, i.e. $T_R = 1250$ °C. However, it should be emphasized that using any temperature in the range from 1000 to 1250 °C does not significantly alter the results obtained here.

TABLE I Coefficient of thermal expansion (CTE), Young's modulus and Poisson's ratio of Al_2O_3 and SiC as a function of temperature

	Al_2O_3	SiC
CTE ($10^{-6}\,°C^{-1}$)	$\alpha_m = 7.04 + 3.92\times10^{-3}\,T - 0.66\times10^{-6}\,T^2$ [a]	$\alpha_p = 3.53 + 2.91\times10^{-3}\,T - 0.64\times10^{-6}\,T^2$ [b]
Young's modulus	$E_m = 410[1 - 1.25\times10^{-4}(T - 25)]$ [c] (GPa)	$E_p = 440[1 - 0.45\times10^{-4}(T - 25)]$ [d] (GPa)
Poisson's ratio	$\nu_m = 0.23[1 + 0.56\times10^{-4}(T - 25)]$ [c]	$\nu_p = 0.17[1 - 0.64\times10^{-4}(T - 25)]$ [e]

T temperature measured in °C.
[a] (25–1600 °C) [13].
[b] (25–2500 °C) [13].
[c] (25–1300 °C) [14].
[d] (25–1000 °C) [15].
[e] calculated using $\nu = E/2G - 1$ where G is the shear modulus.

Clearly, the residual stresses increase with decreasing distance from the particle, and reach a maximum value at the interface between the matrix and the particle ($r = R$)

$$(\sigma_{rr})_{r=R} = -2(\sigma_{\theta\theta})_{r=R} = \int_T^{T_R} \frac{\alpha_m - \alpha_p}{(1+\nu_m)/2E_m + (1-2\nu_p)/E_p}\,dT \quad (2)$$

According to Von Mises's criterion, yielding will occur when τ_{res}, the maximum shear stress, due to the residual stresses exceeds the yield stress

$$\tau_{res} = \frac{1}{2^{\frac{1}{2}}}[(\sigma_{xx}-\sigma_{yy})^2 + (\sigma_{yy}-\sigma_{zz})^2 + (\sigma_{zz}-\sigma_{xx})^2 + 6(\tau_{xy}^2 + \tau_{yz}^2 + \tau_{zx}^2)]^{1/2} \quad (3)$$

where σ_{xx}, σ_{yy} and σ_{zz} are normal stresses, and τ_{xy}, τ_{yz} and τ_{zx} shear stresses. For a three-dimensional spherical particle in the matrix

$$\sigma_{xx} = (\sigma_{rr})_{r=R} \qquad \sigma_{yy} = \sigma_{zz} = (\sigma_{\theta\theta})_{r=R}$$
$$\tau_{xy} = \tau_{yz} = \tau_{zx} = 0 \quad (4)$$

Substituting from Equations 4 and 2 into Equation 3 results in the following simple form for the maximum residual shear stress

$$\tau_{res} = \frac{3}{2}(\sigma_{rr})_{r=R} = \frac{3}{2}\int_T^{T_R} \frac{\alpha_m - \alpha_p}{(1+\nu_m)/2E_m + (1-2\nu_p)/E_p}\,dT \quad (5)$$

Fig. 1 shows the maximum residual shear stress τ_{res} as a function of temperature in the Al_2O_3 matrix for a Al_2O_3/SiC composite. The results take into account the dependence of α, ν and E on temperature, and were calculated using a numerical method. For comparison, Fig. 1 also includes the temperature dependence of the yield stress required for basal and prismatic slip, and for the rhombohedral twinning in Al_2O_3 [22]. Three features are evident from the figure: (1) over all temperatures, the residual shear stress is always less than the yield stress for prismatic slip; (2) for most temperatures, the residual shear stress is higher than the yield stress for rhombohedral twinning; and (3) for temperatures ranging from about 900 to 1100 °C, the residual shear stress is higher than the yield stress for basal slip.

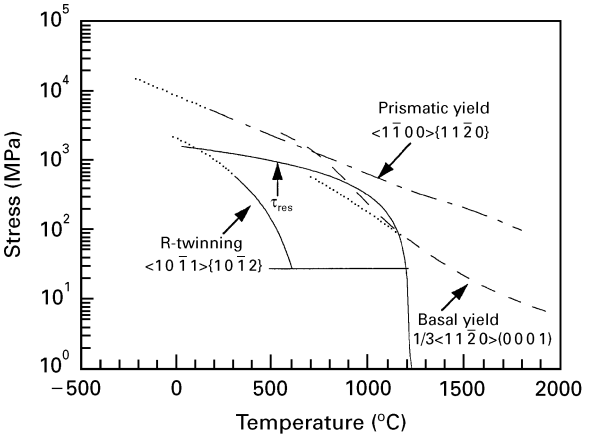

Figure 1 Graph showing the calculated temperature dependence of the maximum residual shear stress τ_{res} in the Al_2O_3 matrix due to thermal expansion mismatch for the Al_2O_3/SiC nanocomposite. Included also is the temperature dependence of the yield stress required for basal and prismatic slip, and for rhombohedral twinning in Al_2O_3 [22].

The important point here is that the magnitude of the maximum residual shear stress is great enough to induce basal slip, but not sufficient to activate the prismatic slip systems in the Al_2O_3 matrix. Since there are only two independent basal slip systems, it is not possible to satisfy the criterion (greater than or equal to five independent slip systems) for extensive plastic deformation in polycrystalline materials. In other words, the level of the residual stresses is such that the amount of plastic deformation is limited, and consequently, it is unlikely that an extensive subgrain structure would be formed in the nanocomposite.

The magnitude of the residual stress calculated using the above theoretical analysis is consistent with the experimental measurement by Levin *et al.* [23]. Clearly from the considerations of force equilibrium at the particle–matrix interface, the compressive stress within the SiC particle must be equal to the radial compressive stress $(\sigma_{rr})_{r=R}$ in the Al_2O_3 matrix. The value of $(\sigma_{rr})_{r=R}$ was calculated from Equation 2 to be 1740 MPa, which is in good agreement with the measured value (about 1780 MPa) of the residual thermal stress inside SiC in 12 vol % SiC–Al_2O_3 nanocomposite [23].

3.2. TEM characterization of bulk microstructure

To test the validity of the above theoretical calculation, TEM was used to characterize the microstructure of both hot-pressed and pressureless sintered 5 vol % SiC–Al_2O_3 nanocomposites. Similar results were obtained in both materials.

Fig. 2a shows a typical TEM micrograph depicting SiC particles ranging from 10 nm to 200 nm dispersed within the Al_2O_3 matrix. While the majority of particles were located within the grains, some particles were present at the grain boundaries. In most areas, no deformation structure was observed. In some isolated areas, dislocations were present (Fig. 2b) but the overall density was very low.

Fig. 3a shows a bright-field image of a dislocation network in the composite. The network consisted of many apparently single perfect dislocations with the majority of dislocations having the same line orientation. Elastic distortion caused by residual stresses due to the thermal expansion mismatch precluded analysis of the Burger's vector of the dislocations. However, the feature of dislocations parallel to $[1\,1\,\bar{2}\,0]$ in Fig. 3a suggests that the dislocations within the network are screw dislocations generated by basal slip.

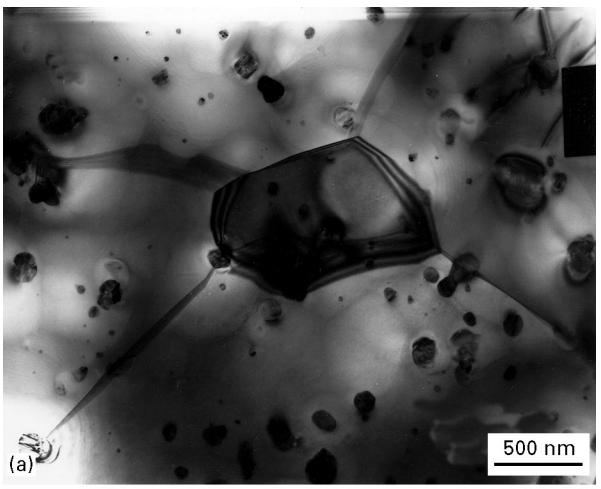

Figure 2 TEM bright-field images of 5 vol % SiC–Al_2O_3 nanocomposite showing the absence of deformation structure in most areas (a) and the presence of a low density of dislocations in isolated regions (b).

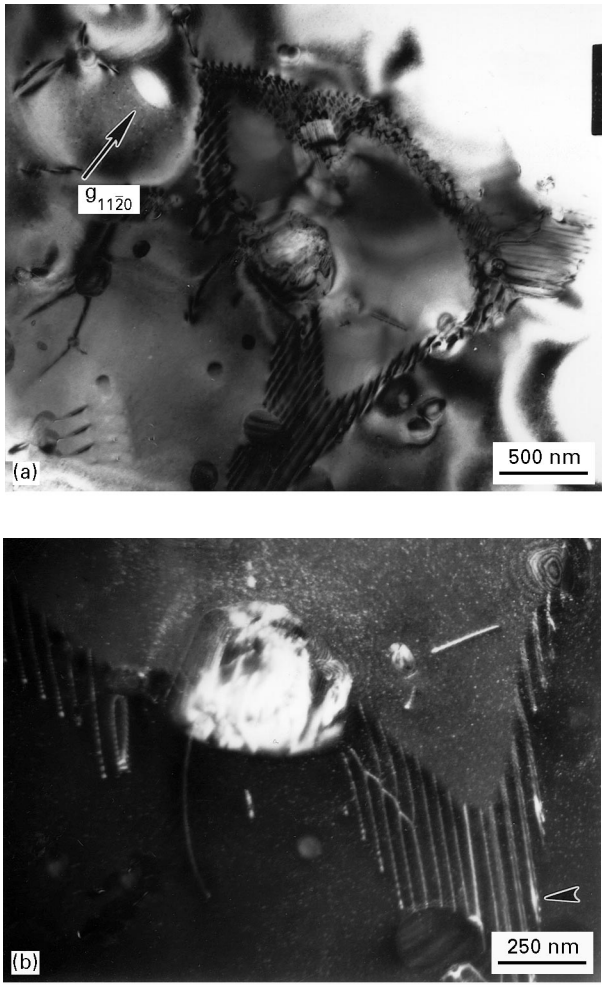

Figure 3 (a) showing bright-field image of dislocation network in the nanocomposite. The beam direction is [0 0 0 1]. Higher magnification weak-beam image (b) revealed that some dislocations were dissociated into a pair of partial dislocations.

Similar dislocation configurations have also been observed in sapphire single crystals deformed by shock-loading [24]. These TEM observations are consistent with the results established in some earlier work [25–27] that slip in Al_2O_3 occurs more easily on the $1/3\langle 1\,1\,\bar{2}\,0\rangle\{0\,0\,0\,1\}$ systems.

Some apparently single dislocations are resolved into pairs of partial dislocations under weak-beam imaging (as arrowed in Fig. 3b). No attempt was made here to identify the nature of these partial dislocations. One possible dissociation was suggested by Kronberg [28] as follows

$$1/3[1\,1\,\bar{2}\,0] \rightarrow 1/3[1\,0\,\bar{1}\,0] + \text{faulted structure} + 1/3[0\,1\,\bar{1}\,0]$$

Here, $1/3\langle 1\,0\,\bar{1}\,0\rangle$ vector corresponds to single oxygen–oxygen distance in a direction of closest packing. To confirm this dislocation dissociation, detailed dislocation analysis (Burgers' vector, dislocation line orientation and faulted structure) would be necessary.

In rare instances, examples of twinned alumina grains were observed (see Fig. 4). Selected area diffraction (SAD) revealed that the twin plane was $(1\,0\,\bar{1}\,2)$, indicating that these twins were of the rhombohedral character. At first sight, the fact that twinning was rarely observed would seem to be inconsistent with

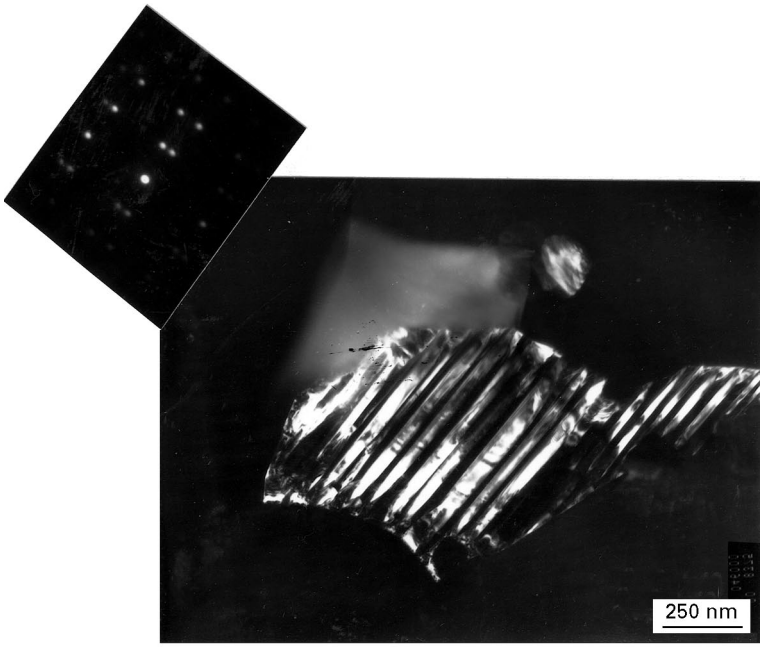

Figure 4 Weak-beam micrographs from the nanocomposite showing rhombohedral twins and selected-area diffraction pattern.

the theoretical calculation that the maximum shear residual stress is about 15 times higher than the yield stress required for rhombohedral twinning. However, in the nanocomposite, because the stresses decrease very rapidly with distance, the high level of residual thermal stresses is limited to small areas close to the matrix/particle interface. This means that, in the bulk of the Al_2O_3 grains, the thermal residual stress is much lower than the stress required for twinning.

For the bulk nanocomposite materials (both unannealed and annealed), nowhere were any subgrains observed. This agrees with other published work [6, 29] on Al_2O_3–5 vol % SiC nanocomposites. It is thus concluded that microstructure refinement through subgrain formation in these materials [7, 8] does not occur, and hence is not responsible for the superior mechanical behaviour of the nanocomposite.

3.3. Microstructure of ground surface

Fig. 5a and b show the deformation structure of the ground surfaces in Al_2O_3 and in the nanocomposite, respectively. Note the high densities of dislocations produced during grinding at room temperature, indicating that both materials have been subjected to severe deformation. The addition of SiC particles did not have an observable effect on the deformation structure. The characteristic feature of the deformation structure was that the majority of dislocations was limited to narrow linear bands delineating the traces of the surface scratches. The density of dislocations within the scratches was so high that individual dislocations were barely resolvable. In the present study, Burger's vector analysis could not be carried out due to the severe bending in the TEM samples. However, Hockey [30] reported similar deformation structures for polycrystalline Al_2O_3 subjected to grinding, and showed that slip occurred on both the basal and non-basal planes.

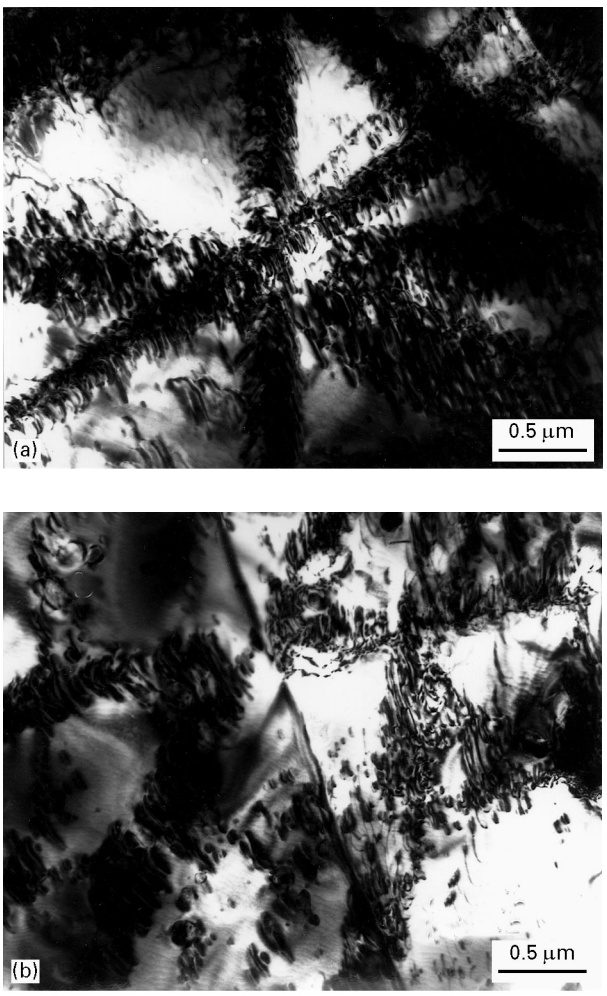

Figure 5 TEM micrographs showing deformed structure on the machined surface in (a) Al_2O_3 and (b) nanocomposite.

Annealing resulted in different structures in the two materials. For Al_2O_3(Fig. 6a), dislocation-free subgrains were observed in most areas; occasionally, however, dislocation cells, within which the dislocation

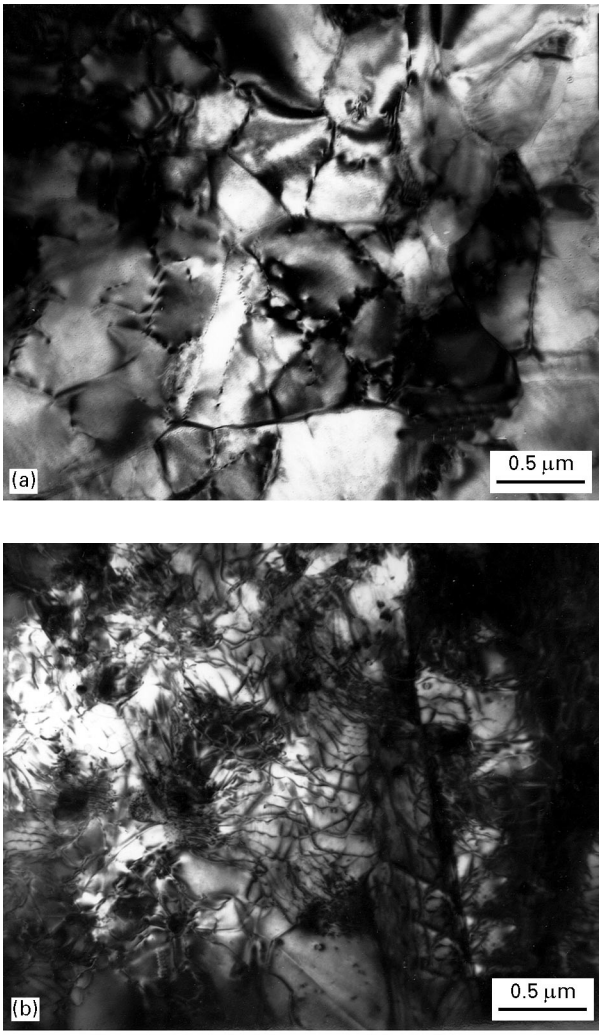

Figure 6 TEM micrographs showing that annealing resulted in (a) dislocation-free subgrains for the machined surface in Al_2O_3, but (b) a high density of dislocations in the nanocomposite.

densities were very low, were formed. However, for the nanocomposite, the microstructure consisted of a high density of tangled dislocations and a few scattered dislocation cells (Fig. 6b).

We believe that in Al_2O_3 dislocations are able to move away from the heavily deformed areas and rearrange to form networks. During prolonged annealing, these networks evolve into cells or subgrains. In contrast, in the nanocomposite, the SiC particles inhibit dislocation motion and rearrangement, and retard dislocation cell/subgrain formation. A similar retarding effect of particles on recrystallization has been reported in many metal systems such as Al–5 vol % 0.3 μm Al_2O_3 [31] and Ni–2 vol % 0.1 μm ThO_2 [32]. These observations provide microscopic evidence which confirms the results of previous studies [4, 10, 33], namely that annealing completely relaxes surface residual stresses in Al_2O_3, but only partially relieves the stresses in the nanocomposite.

4. Conclusions

1. Calculations showed that the maximum residual shear stress due to thermal expansion mismatch between Al_2O_3 and SiC is greater than the yield stress for both basal slip and rhombohedral twinning, but smaller than that for prismatic slip. Since there are only two independent basal slip systems, extensive plastic deformation, which is required for subgrain formation, is not possible.

2. Within the interior of the nanocomposite, a very low density of apparently basal dislocations was observed. Occasionally, rhombohedral twins were present. Nowhere were any sub-grains observed. Therefore, the improved mechanical behaviour of the nanocomposite cannot arise from microstructure refinement through sub-grain formation.

3. The ground surfaces contained very high densities of dislocations in both single phase Al_2O_3 and the nanocomposite. Upon annealing at 1300 °C for 2 h, the surface microstructure was predominantly characterized by a large number of dislocation-free subgrains/cells in Al_2O_3, and by a high density of tangled dislocations in the nanocomposite. This microstructure difference is reflected macroscopically in the fact that annealing completely relaxes the surface residual stresses in Al_2O_3, but only partially relieves the stresses in the nanocomposite.

Acknowledgements

The authors wish to thank L. C. Stearns and J. Zhao for providing the specimens. This research was sponsored by the US Office of Naval Research under contract N00014-92-J-1635, and by the Electric Power Research Institute under contract RP2426-54.

References

1. K. NIIHARA and A. NAKAHIRA, in Proceedings of the Third International Symposium on Ceramic Materials & Components for Engines (The American Ceramic Society, Westerville, OH, 1988) p. 919.
2. K. NIIHARA, A. NAKAHIRA, G. SASAKI and M. HIRABAYASHI, in Proceedings of the International Meeting on Advanced Materials, vol. 4 (The Materials Research Society, Japan, 1989) p. 124.
3. K. NIIHARA and A. NAKAHIRA, "Advanced structural inorganic composites", edited by P. Vincenzini (Elsevier Science Publishers, Trieste 1990) p. 637.
4. J. ZHAO, L. C. STEARNS, M. P. HARMER, H. M. CHAN, G. A. MILLER and R. F. COOK, *J. Amer. Ceram. Soc.* **76** (1993) 503.
5. I. LEVIN, W. D. KAPLAN, DAVID G. BRANDON and A. A. LAYYOUS, to be published.
6. HANS WOHLFROMM, *Ceram. Trans.* **51** (1994) 659.
7. K. NIIHARA, *J. Ceram. Soc. Japan* **99** (1991) 974.
8. K. NIIHARA, A. NAKAHIRA and T. SEKINO, *Mater. Res. Soc. Symp. Proc.* **286** (1993) 405.
9. A. M. THOMPSON, H. M. CHAN and M. P. HARMER, *J. Amer. Ceram. Soc.* **78** (1994) 567.
10. J. FANG, H. M. CHAN and M. P. HARMER, *Mater. Sci. Eng.* **A195** (1995) 163.
11. L. C. STEARNS, J. ZHAO and M. P. HARMER, *J. Eur. Ceram. Soc.* **10** (1992) 473.
12. J. SELSING, *J. Amer. Ceram. Soc.* **44** (1961) 419.
13. Y. S. TOULOUKIAN, R. K. KIRBY, R. E. TAYLOR and T. Y. R. LEE (eds) "Thermophysical properties of matter", Vol. 13, (IFI/Plenum, New York, 1970).
14. R. MORRELL (ed) "Handbook of properties of technical & engineering ceramics", Part 2 Data Reviews, Section 1 High-Alumina Ceramics, (Her Majesty's Stationery Office, London, 1987).

15. H. C. CHANDAN, Ph.D. Dissertation, Pennsylvania State University (1980).
16. Z. LI and R. C. BRADT, *J. Amer. Ceram. Soc.* **72** (1989) 70.
17. A. ABUHASAN, C. BALASINGH and P. PREDECKI, *ibid.* **73** (1990) 2474.
18. C. N. TOMÉ, M. A. BERTINETTI and S. R. MacEWEN, *ibid.* **73** (1990) 3428.
19. I. LEVIN, W. D. KAPLAN, D. G. BRANDON and A. A. LAYYOUS, *ibid.* **78** (1995) 254.
20. S. MAJUMDAR, D. KUPPERMAN and J. SINGH, *ibid.* **71** (1988) 858.
21. S. MAJUMDAR and D. KUPPERMAN, *ibid.* **72** (1989) 312.
22. R. M. CANNON, in "Structure and properties of MgO and Al_2O_3 ceramics", Advances in Ceramics Vol. 10, edited by W. D. Kingery (The American Ceramic Society, Inc., Westerville, OH, 1984) p. 818.
23. I. LEVIN, W. D. KAPLAN, D. G. BRANDON and T. WIEDER, *Acta Metall.* **42** (1994) 1147.
24. Y. WANG and D. E. MIKKOLA, *J. Amer. Ceram. Soc.* **75** (1992) 3252.
25. J. B. WACHTMAN, Jr. and L. H. MAXWELL, *ibid.* **37** (1954) 291.
26. *Idem.*, *ibid.* **40** (1957) 377.
27. M. L. KRONBERG, *ibid.* **45** (1962) 274.
28. *Idem. Acta Metall.* **5** (1957) 507.
29. M. RÜHLE, private communication (1995).
30. B. HOCKEY, *J. Amer. Ceram. Soc.* **54** (1971) 223.
31. E. J. WESTERMAN and F. V. LENEL, *Trans. Met. Soc. AIME* **218** (1960) 1010.
32. M. C. INMAN, K. M. ZWILSKY and D. H. BOONE, *Trans. Amer. Soc. Metals* **57** (1964) 701.
33. I. CHOU, H. M. CHAN and M. P. HARMER, *J. Amer. Ceram Soc.* **79** (1996) 2403.

Received 19 April
and accepted 13 November 1996